



# Thermal Modelling and Analysis of A 10HP Induction Machine Using the Lumped Parameter Approach

Oti S.Ejiofor<sup>1\*</sup>, Awah Chukwemeka<sup>2</sup>, Chibuzo Nnonyelu<sup>1</sup>, Ogonnaya I.Okoro<sup>2</sup>

<sup>1</sup>Department of Electrical Engineering,  
University of Nigeria, Nsukka, Enugu State, NIGERIA

<sup>2</sup>Department of Electrical/Electronic Engineering, Michael Okpara  
University of Agriculture, Abia State, NIGERIA

\*Corresponding Author

DOI: <https://doi.org/10.30880/ijie.2021.13.06.016>

Received 24 December 2019; Accepted 12 May 2020; Available online 31 August 2021

**Abstract:** The essence of this research work is to develop a thermal model for an induction machine that will enable the prediction of temperature in different parts of the machine. This is very important first to the manufacturer or designer of an induction machine because with these predictions one can decide on the insulation class limits the machine belongs to. Also modern trends in the construction of machines is moving in the direction of making machines with reduced weights, costs and increased efficiency. In order to achieve this, the thermal analysis becomes very crucial in deciding on what types of insulators and other materials that would be used to make these machines. In industries, the knowledge of the thermal limits of machines if well utilized increases the life span of the machines and reduces downtime; thereby increasing production and profit. Specifically, this paper (i) predicted the temperature limits of the induction machine and its components, (ii) developed an accurate thermal model for an induction machine, (iii) predicted the temperature in different parts of the induction machine using the thermal model and software program and lastly (iv) investigated how the machine symmetry is affected by the nodal configuration.

**Keywords:** Thermal, transient, induction, temperature, lumped

## 1. Introduction

The work is concerned with the thermal modelling and analysis of the induction machine, a vital aspect of research that many authors [1-10] have made numerous attempts at studying. In the design of the induction machines, the manufacturers take many factors into consideration to ensure that it works efficiently. An outstanding factor of much concern is its thermal limits for different operating conditions since, working much away from its thermal limit for a reasonable length of time can cause the machine's life span to reduce drastically. The malfunctioning of a motor due to unnecessary heating may apart from posing service delivery constraint, cause immense financial losses due to unexpected process downtime. Approximately one-third of machine failures are not unconnected to failure resulting from winding insulation. Machines used in industries today are banking on electromechanical and thermal instruments as escape means during overloading but thermal overheating contributes a lot towards the degradation [11]. As thermal overload spells out as a principal agent in cases of winding insulation failure, there is need for prompt attention to be given to the design that will bring about reduction in such damages that lead to motor breakdown, and consequent reduction of one's financial base due to unanticipated process downtime. The practice of adopting motor control devices of variable frequency schemes with reduced motor current starters has put the control and progress of thermal protection in the lime light, hence promoting the overall applicability to efficient machine control thereby increasing

\*Corresponding author: [stephen.oti@unn.edu.ng](mailto:stephen.oti@unn.edu.ng)

2021 UTHM Publisher. All rights reserved.

[penerbit.uthm.edu.my/ojs/index.php/ijie](http://penerbit.uthm.edu.my/ojs/index.php/ijie)

the desirability. This afore mentioned schemes become more viable with thermal model of this kind which integrated the rotor and stator teeth which were usually not considered by many past researchers. The main aim of this work is to develop a thermal model of the squirrel cage induction machine (SCIM) using the lumped parameter model. The thermal network models, (TNM) [12-15] popularly called the lumped parameter model is one of the schemes adopted in studying thermal models for the determination of rise in temperature in electrical machines. The finite element method (FEM) has also been used by many authors [16,17] to determine temperature rise in electrical systems but the lumped-parameter thermal method (LPTM) is the approach used here because, apart from being easier and accurate, it can be adapted to different frame sizes. Many fabricators of Electrical machine employ the computational fluid dynamics (CFD) packages in flow and cooling modelling [18], and make use of them even in the thermal control of ac motors [19]. The thermal model developed is based on thermal resistances, thermal capacitances and power losses and it is structured as small induction machine (SIM) and large induction machine (LIM) models so that the effect of the nodal configuration on the machine symmetry can be investigated. Optimum level of prudence is employed in dividing and adopting of machine parts as according to [20], such practice will be free of over simplicity and over complication in an attempt to be very thorough.

### 1.1 Heat Balance Equations

In the lumped parameter thermal circuit analysis, it is often assumed that the temperature gradient with certain parts of the machine is negligible. According to [21] this assumption can only be made if the internal resistance to the heat transfer is small compared with the external resistance. The Biot number  $B_i$ , is usually used for determining the validity of this assumption. In the case where internal conduction resistance is compared with external convective resistance,  $B_i$  is defined as:  $B_i = \frac{h_c L}{k_s}$  Where ‘ $k_s$ ’ is the thermal conductivity of the solid material, ‘ $L$ ’ is the characteristic length of the solid body and ‘ $h_c$ ’ is the convective heat transfer coefficient. The criterion  $B_i < 0.1$  ensures that the internal temperature will not differ and according to [22], at the onset of the step change, one can assume a uniform temperature which for such, the time for the change is confined in a thin ‘skin’ near the fluid or solid surface.

### 1.2 Thermal Models and Network Theory

In modelling a thermal network, the material is discretized giving rise to aggregates of thermal elements that join at a given node through thermal resistances. Inadequate discretization has been considered in [23] as one source of discrepancies between experimental and simulated results. When duly considered, the thermal network so formed can be likened to electrical network as detailed in [14, 15]. The simplified diagrams of figures (1) and (2) below depict a generalized thermal model as proposed in this paper.

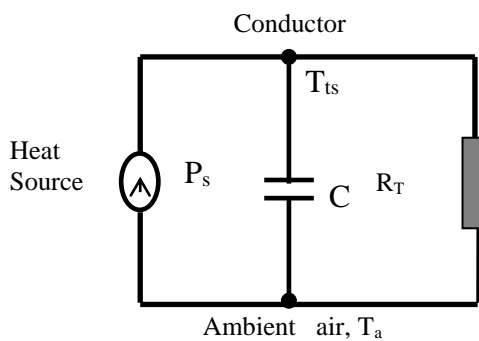


**Fig. 1 - Transient Thermal model of SCIM with lumped parameter**

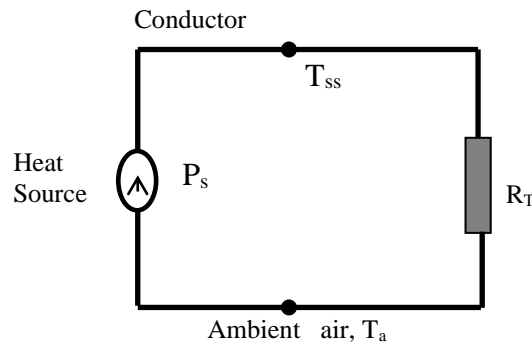


**Fig. 2 - Steady State Thermal model of SCIM with lumped parameter**

If the conductor temperature rise  $\Delta T$  is considered as the rise in relation to ambient temperature  $T_a$  caused by the presence of heating loss  $P_s$ , then the temperature rise is generally given by the final temperature  $T_f$  minus the initial temperature. In this case, the ambient temperature  $T_a$  is the initial value, therefore,  $\Delta T = T_f - T_a$  (1)

In Figure 1, the model for the transient state is presented and the change in temperature is represented as  $\Delta T_{ts}$  so that  $\Delta T_{ts} = T_{ts} - T_a$ . In like manner, in Figure 2, the model for the steady state is presented and the change in temperature is represented as  $\Delta T_{ss}$  so that  $\Delta T_{ss} = T_{ss} - T_a$ . On recall, any resistor on the same branch of a circuit as a capacitor receives no current, and therefore does not lose any voltage. At steady state, the capacitor becomes charged and acts like an open circuit, therefore, at steady state, the model of Figure 2, going by Kirchoff's law would be

represented by  $P_s = \frac{\Delta T_{ss}}{R_T}$ . However, the transient state of Figure 1 has additional capacitive component hence the model's power loss is represented as  $P_s = \frac{\Delta T_{ts}}{R_T} + C \frac{d\Delta T}{dt}$ . In general terms, the temperature rise irrespective of the model type is denoted as  $\Delta T$ ; this will thus give  $C \frac{d\Delta T}{dt} + \frac{\Delta T}{R_T} - P_s = 0$ . (2)

The ambient air temperature  $T_a$ , serves as the thermal reference while a deviation from the reference, that is, a rise in temperature denotes the machine elements. Assuming that we have 'N' number of nodes singly linked to other nodes via thermal resistances  $R_{a,b}$  in which 'a' and 'b' are the number of the nodes, with  $R_{a,b}$  as the thermal resistance between the reference and node 'b' then the steady-state rise in temperature at the node 'a' can be derived from the relation:  $0 = P_a - \frac{T_a}{R_{a,b}} + \sum_{b=1}^N \left( \frac{T_b}{R_{a,b}} \right)$  a = 1 (3)

Where  $P_a$  = the heat generation at node a,  $T_a$  = the temperature of node a  
 $R_{a,b}$  = thermal resistance between two adjoining nodes a and b.

For multi- node consideration,  $T_1$  to  $T_N$  represent the temperature rises of each node while  $P_1$  to  $P_N$  represent the losses at the various nodes. The matrix defined by 'G' in equation (4) is a conductance matrix which when joined with the column vectors represented by  $P_T$  and  $T_T$  as given below give rise to equation (5) which leads to a stationary solution using equation (6).

$$G = \begin{bmatrix} \sum_{a=1}^N \frac{1}{R_{1,a}} & -\frac{1}{R_{1,2}} & -\frac{1}{R_{1,3}} & -\frac{1}{R_{1,4}} & \dots & -\frac{1}{R_{1,N}} \\ -\frac{1}{R_{2,1}} & \sum_{a=1}^N \frac{1}{R_{2,a}} & -\frac{1}{R_{2,3}} & -\frac{1}{R_{2,4}} & \dots & -\frac{1}{R_{2,N}} \\ \dots & \dots & \dots & \dots & \dots & \dots \\ -\frac{1}{R_{N,1}} & -\frac{1}{R_{N,2}} & -\frac{1}{R_{N,3}} & -\frac{1}{R_{N,4}} & \dots & \sum_{a=1}^N \frac{1}{R_{N,a}} \end{bmatrix} \quad (4)$$

with  $P_T$  represented as  $[P_1 \ P_2 \ \dots \ P_N]^{-1}$  and  $T_T$  taken as  $[T_1 \ T_2 \ \dots \ T_N]^{-1}$  we have that  $P_T = GT_T$  (5)

which modifies to  $T_T = G^{-1}P_T$  (6)

The SIM thermal network in full form as shown in figure (3) has a total of twelve nodes and fifteen thermal resistances, while that of LIM as shown in figure (4) has fourteen nodes and eighteen thermal resistances. It was assumed in [19] that the heat transferred from the rotor winding through the air-gap goes directly to the stator winding with negligible impact on the stator teeth, however this assumption did not go down well with the LIM model here as the teeth is fully considered and the effects studied alongside others. Hence, the rotor part of the machine is divided into the rotor iron, rotor windings, rotor teeth and end rings while the stator of the machine has networks for the stator iron, stator winding, and end winding together with the stator teeth. The connection of the above mentioned networks for rotor, stator and frame gives rise to the thermal network models of figures (3 and 4) as shown below. A node is all the points in a circuit that are directly interconnected. We assume the interconnections have zero resistance, so all points within a node have the same temperature. The aim of nodal analysis is to determine the temperature at each node relative to the reference node. The separate temperatures of the nodes are evaluated using this set of heat balance equation as given below.

$$C_a \frac{dT}{dt} = P_a - \left( \frac{1}{R_{ab}} (T_a - T_b) \right) \quad a, b = 1 \quad (7)$$

Where  $C_a$  = thermal capacitance of node a,  $T_a$  = the temperature of node 'a';  $R_{ab}$  = thermal resistance between two adjoining nodes 'a' and 'b';  $P_a$  = the heat generation at node 'a'. The power losses ( $P_1 - P_{11}$ ) associated with the model of figure (3) are outlined in equations (8 – 20). However, in the simulation for the half model of the induction machine, equations (8 – 15) representing ( $P_1$ ) to ( $P_8$ ) are used. This is equivalent to losses equations ( $P_1 - P_8$ ) and are shown at the right hand side of figure (3) with shaded resistors.

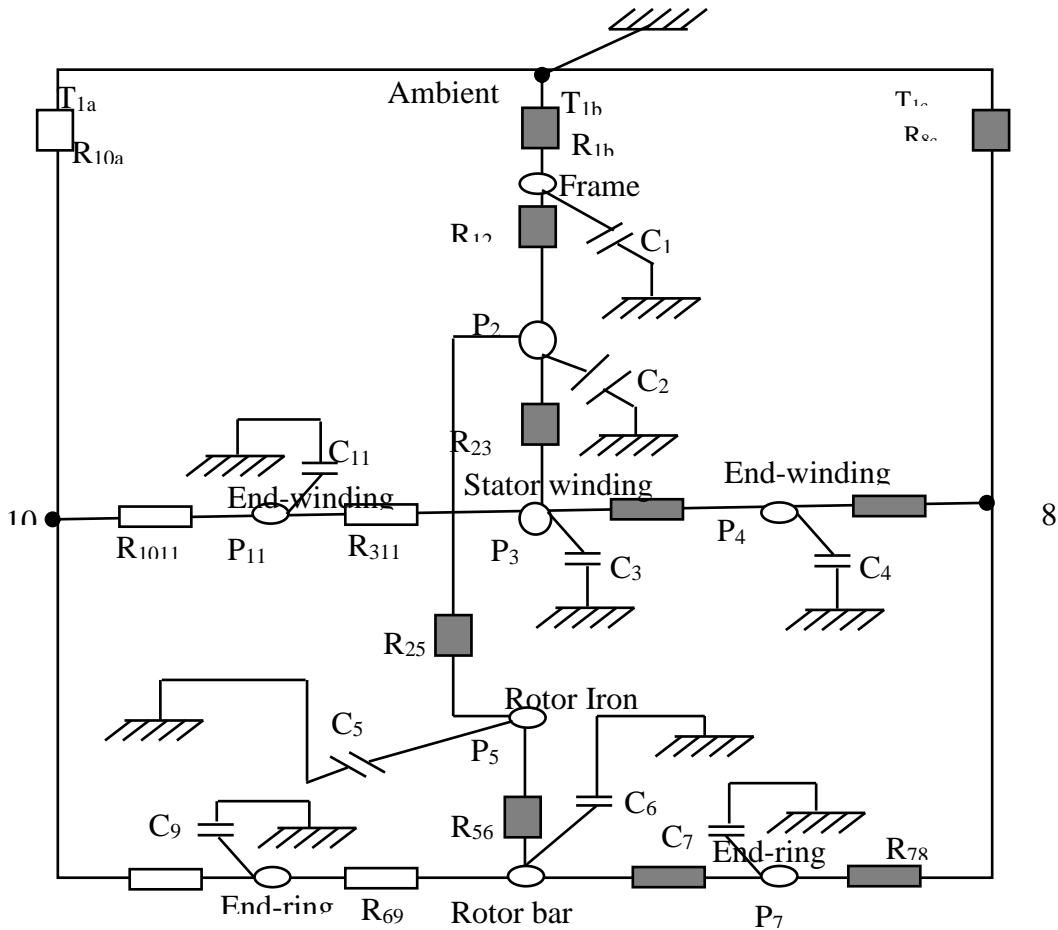


**Fig. 3 - Thermal network for the squirrel cage induction machine with SIM Half Model considered**

In the case of the complete (LIM) model, equations (16 and 17) for ( $P_3$ ) and ( $P_6$ ) are respectively modified as ( $P'_3$ ) and ( $P'_6$ ) while equations (18 – 20) for ( $P_9$ ), ( $P_{10}$ ) and ( $P_{11}$ ) as derived from the complete model are added so as to

$$P_1 = C_1 \frac{dT_1}{dt} + \frac{1}{R_{12}}(T_1 - T_2) + \frac{1}{R_{1b}}(T_1 - T_b) \tag{8}$$

$$P_2 = C_2 \frac{dT_2}{dt} + \frac{1}{R_{12}}(T_2 - T_1) + \frac{1}{R_{23}}(T_2 - T_3) + \frac{1}{R_{25}}(T_2 - T_5) \tag{9}$$

$$P_3 = C_3 \frac{dT_3}{dt} + \frac{1}{R_{32}}(T_3 - T_2) + \frac{1}{R_{34}}(T_3 - T_4) \tag{10}$$

$$P_4 = C_4 \frac{dT_4}{dt} + \frac{1}{R_{48}}(T_4 - T_8) + \frac{1}{R_{34}}(T_4 - T_3) \tag{11}$$

$$P_5 = C_5 \frac{dT_5}{dt} + \frac{1}{R_{52}}(T_5 - T_2) + \frac{1}{R_{56}}(T_5 - T_6) \tag{12}$$

$$P_6 = C_6 \frac{dT_6}{dt} + \frac{1}{R_{65}}(T_6 - T_5) + \frac{1}{R_{67}}(T_6 - T_7) \tag{13}$$

$$P_7 = C_7 \frac{dT_7}{dt} + \frac{1}{R_{76}}(T_7 - T_6) + \frac{1}{R_{78}}(T_7 - T_8) \tag{14}$$

$$P_8 = C_8 \frac{dT_8}{dt} + \frac{1}{R_{87}}(T_8 - T_7) + \frac{1}{R_{84}}(T_8 - T_4) + \frac{1}{R_{8c}}(T_8 - T_c) \tag{15}$$

$$P'_3 = C_3 \frac{dT_3}{dt} + \frac{1}{R_{32}}(T_3 - T_2) + \frac{1}{R_{34}}(T_3 - T_4) + \frac{1}{R_{311}}(T_3 - T_{11}) \tag{16}$$

$$P'_6 = C_6 \frac{dT_6}{dt} + \frac{1}{R_{65}}(T_6 - T_5) + \frac{1}{R_{67}}(T_6 - T_7) + \frac{1}{R_{69}}(T_6 - T_9) \tag{17}$$

$$P_9 = C_9 \frac{dT_9}{dt} + \frac{1}{R_{69}}(T_9 - T_6) + \frac{1}{R_{910}}(T_9 - T_{10}) \tag{18}$$

$$P_{10} = C_{10} \frac{dT_{10}}{dt} + \frac{1}{R_{1011}}(T_{10} - T_{11}) + \frac{1}{R_{910}}(T_{10} - T_9) + \frac{1}{R_{10a}}(T_{10} - T_a) \tag{19}$$

$$P_{11} = C_{11} \frac{dT_{11}}{dt} + \frac{1}{R_{311}}(T_{11} - T_3) + \frac{1}{R_{1011}}(T_{11} - T_{10}) \tag{20}$$

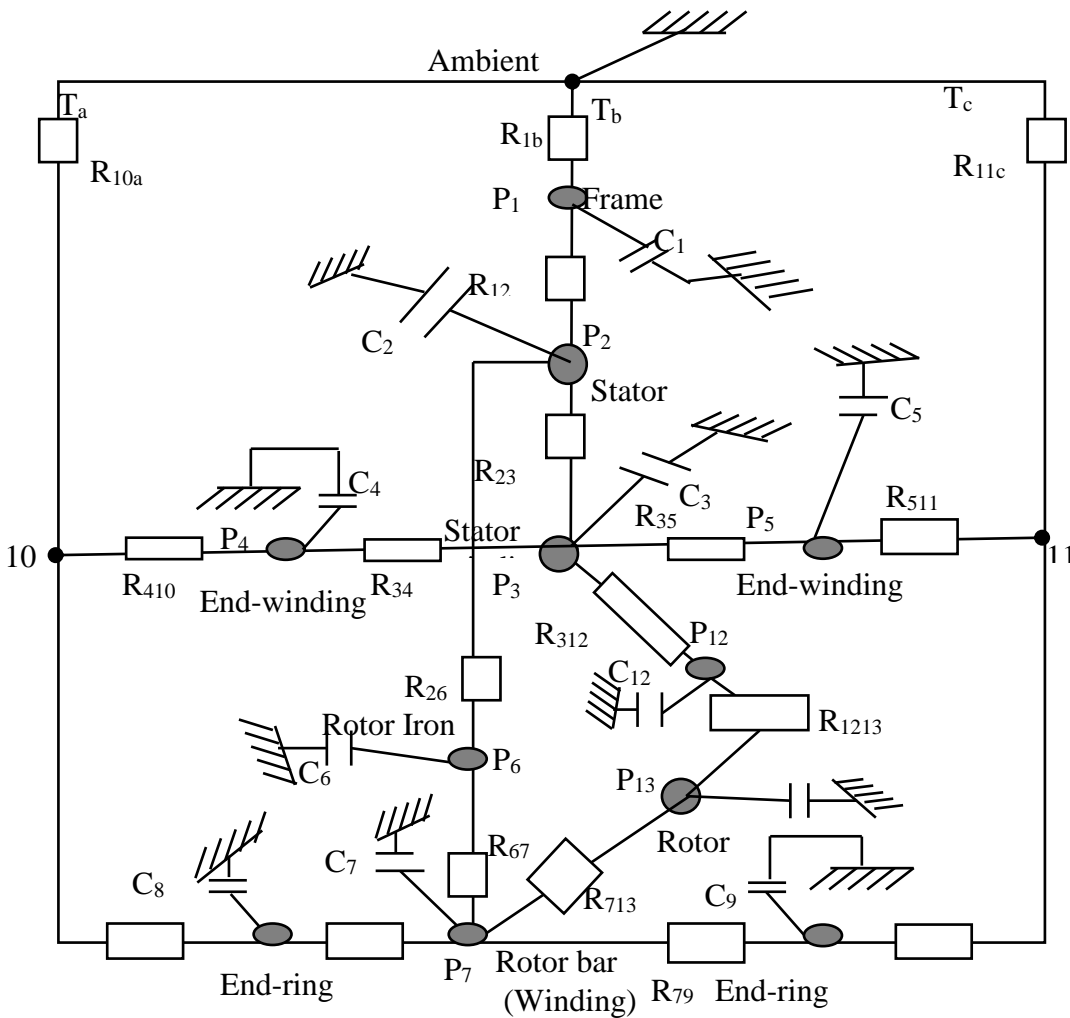


**Fig. 4 - Thermal network model for the squirrel cage induction machine for LIM full model**

## 2. Methodology

### 2.1 The Transient State Analysis

The general transient equation for thermal network system of ‘*N*’ nodes linking others through thermal resistances  $R_{a,b}$  is represented as follows:

$$[C_a] \frac{d[T]}{dt} = P_a - \frac{T_a}{R_{a,b}} + \sum_{b=1}^N \left( \frac{T_b}{R_{a,b}} \right) \quad a = 1 \quad (21)$$

The existence of thermal capacitance in the network demands that a thermal capacitance matrix as given below will be incorporated.

$$C = \begin{bmatrix} C_1 & 0 & 0 & 0 & \dots & 0 \\ 0 & C_2 & 0 & 0 & \dots & 0 \\ \dots & \dots & \dots & \dots & \dots & \dots \\ 0 & 0 & 0 & 0 & \dots & C_N \end{bmatrix} \quad (22)$$

Hence we have,  $[C] \frac{d[T]}{dt} = [P] - [G][T]$  (23)

or  $\frac{d[T]}{dt} = [C]^{-1}[P] - [C]^{-1}[G][T]$  (24)

where

- [C] = column matrix of thermal capacitances
- [G] = square matrix of inter nodal conductance
- [P] = column matrix of thermal generators

The power associated with each thermal node is expressed as can be deduced from equation (21), the system of algebraic and differential equations which emanated from the thirteen nodes sum up the thermal behaviour of the developed thermal model of Figure 4. The constants  $T_a$ ,  $T_b$  and  $T_c$  are the ambient temperature values and are equal, the equations are further rearranged to make each attendant differential the subject as shown below. Matlab programs [20 - 22] are developed to solve the steady state and transient state mathematical models of the machine.

$$\frac{dT_1}{dt} = \frac{1}{C_1} \left[ P_1 - \frac{1}{R_{12}}(T_1 - T_2) - \frac{1}{R_{1b}}(T_1 - T_b) \right] \quad (38)$$

$$\frac{dT_2}{dt} = \frac{1}{C_2} \left[ P_2 - \frac{1}{R_{12}}(T_2 - T_1) - \frac{1}{R_{23}}(T_2 - T_3) - \frac{1}{R_{26}}(T_2 - T_6) \right] \quad (39)$$

$$\frac{dT_3}{dt} = \frac{1}{C_3} \left[ P_3 - \frac{1}{R_{32}}(T_3 - T_2) - \frac{1}{R_{35}}(T_3 - T_5) - \frac{1}{R_{34}}(T_3 - T_4) - \frac{1}{R_{312}}(T_3 - T_{12}) \right] \quad (40)$$

$$\frac{dT_4}{dt} = \frac{1}{C_4} \left[ P_4 - \frac{1}{R_{410}}(T_4 - T_{10}) - \frac{1}{R_{34}}(T_4 - T_3) \right] \quad (41)$$

$$\frac{dT_5}{dt} = \frac{1}{C_5} \left[ P_5 - \frac{1}{R_{53}}(T_5 - T_3) - \frac{1}{R_{511}}(T_5 - T_{11}) \right] \quad (42)$$

$$\frac{dT_6}{dt} = \frac{1}{C_6} \left[ P_6 - \frac{1}{R_{67}}(T_6 - T_7) - \frac{1}{R_{62}}(T_6 - T_2) \right] \quad (43)$$

$$\frac{dT_7}{dt} = \frac{1}{C_7} \left[ P_7 - \frac{1}{R_{67}}(T_7 - T_6) - \frac{1}{R_{78}}(T_7 - T_8) - \frac{1}{R_{79}}(T_7 - T_9) - \frac{1}{R_{713}}(T_7 - T_{13}) \right] \quad (44)$$

$$\frac{dT_8}{dt} = \frac{1}{C_8} \left[ P_8 - \frac{1}{R_{78}}(T_8 - T_7) - \frac{1}{R_{810}}(T_8 - T_{10}) \right] \quad (45)$$

$$\frac{dT_9}{dt} = \frac{1}{C_9} \left[ P_9 - \frac{1}{R_{79}}(T_9 - T_7) - \frac{1}{R_{911}}(T_9 - T_{11}) \right] \quad (46)$$

$$\frac{dT_{10}}{dt} = \frac{1}{C_{10}} \left[ P_{10} - \frac{1}{R_{410}}(T_{10} - T_4) - \frac{1}{R_{810}}(T_{10} - T_8) - \frac{1}{R_{10a}}(T_{10} - T_a) \right] \quad (47)$$

$$\frac{dT_{11}}{dt} = \frac{1}{C_{11}} \left[ P_{11} - \frac{1}{R_{511}}(T_{11} - T_5) - \frac{1}{R_{11c}}(T_{11} - T_c) - \frac{1}{R_{119}}(T_{11} - T_9) \right] \quad (48)$$

$$\frac{dT_{12}}{dt} = \frac{1}{C_{12}} \left[ P_{12} - \frac{1}{R_{312}} (T_{12} - T_3) - \frac{1}{R_{1213}} (T_{12} - T_{13}) \right] \tag{49}$$

$$\frac{dT_{13}}{dt} = \frac{1}{C_{13}} \left[ P_{13} - \frac{1}{R_{713}} (T_{13} - T_7) - \frac{1}{R_{1213}} (T_{13} - T_{12}) \right] \tag{50}$$

Having arranged them in that form, then a matrix form is evolved for them according to this expression shown in equation (51):

$$\begin{bmatrix} \dot{T} \end{bmatrix} = [C_t]^{-1} [P_t] - [C_t]^{-1} * [G_t] [T] \tag{51}$$

where

$$\dot{T} = \begin{bmatrix} \dot{T}_1 & \dot{T}_2 & \dot{T}_3 & \dots & \dot{T}_{13} \end{bmatrix}^{-1} \quad [C_t]^{-1} = \begin{bmatrix} C_1 & 0 & 0 & \dots & 0 \\ 0 & C_2 & 0 & \dots & 0 \\ \dots & \dots & \dots & \dots & 0 \\ 0 & 0 & 0 & \dots & C_{13} \end{bmatrix}^{-1}, \quad T = [T_1 \quad T_2 \quad T_3 \dots T_{13}]^{-1}$$

$$[P_t] = [P_1 + T_b * G_{1b} \quad P_2 \quad P_3 \quad P_4 \quad P_5 \quad P_6 \quad P_7 \quad P_8 \quad P_9 \quad T_a * G_{10a} \quad T_a * G_{11c} \quad P_{12} \quad P_{13}]^{-1}$$

and

$$[G_t] = \begin{bmatrix} G_{11} & -G_{12} & 0 & 0 & 0 & 0 & 0 & 0 & 0 & 0 & 0 & 0 & 0 \\ -G_{21} & G_{22} & -G_{23} & 0 & 0 & -G_{26} & 0 & 0 & 0 & 0 & 0 & 0 & 0 \\ 0 & -G_{32} & G_{33} & -G_{34} & -G_{35} & 0 & 0 & 0 & 0 & 0 & 0 & -G_{312} & 0 \\ 0 & 0 & -G_{43} & G_{44} & 0 & 0 & 0 & 0 & 0 & -G_{410} & 0 & 0 & 0 \\ 0 & 0 & -G_{53} & 0 & G_{55} & 0 & 0 & 0 & 0 & 0 & -G_{511} & 0 & 0 \\ 0 & -G_{62} & 0 & 0 & 0 & G_{66} & -G_{67} & 0 & 0 & 0 & 0 & 0 & 0 \\ 0 & 0 & 0 & 0 & 0 & -G_{76} & G_{77} & -G_{78} & -G_{79} & 0 & 0 & 0 & -G_{713} \\ 0 & 0 & 0 & 0 & 0 & 0 & -G_{87} & G_{88} & 0 & -G_{810} & 0 & 0 & 0 \\ 0 & 0 & 0 & 0 & 0 & 0 & -G_{97} & 0 & G_{99} & 0 & -G_{911} & 0 & 0 \\ 0 & 0 & 0 & -G_{104} & 0 & 0 & 0 & -G_{108} & 0 & G_{1010} & 0 & 0 & 0 \\ 0 & 0 & 0 & 0 & -G_{115} & 0 & 0 & 0 & -G_{119} & 0 & G_{1111} & 0 & 0 \\ 0 & 0 & -G_{123} & 0 & 0 & 0 & 0 & 0 & 0 & 0 & 0 & G_{1212} & -G_{1213} \\ 0 & 0 & 0 & 0 & 0 & 0 & -G_{137} & 0 & 0 & 0 & 0 & -G_{1312} & G_{1313} \end{bmatrix} \tag{52}$$

Some of the entries of the  $G_t$ -matrix are given as follows:

$$G_{11} = G_b + G_{12} \tag{53}$$

$$G_{22} = G_{21} + G_{23} + G_{26} \tag{54}$$

$$G_{33} = G_{32} + G_{35} + G_{34} + G_{312} \tag{55}$$

$$G_{44} = G_{410} + G_{34} \tag{56}$$

$$G_{55} = G_{53} + G_{511} \tag{57}$$

$$G_{66} = G_{67} + G_{62} \tag{58}$$

$$G_{77} = G_{76} + G_{78} + G_{79} + G_{713} \tag{59}$$

$$G_{88} = G_{87} + G_{810} \tag{60}$$

$$G_{99} = G_{97} + G_{911} \tag{61}$$

$$G_{1010} = G_{104} + G_{108} + G_{10a} \tag{62}$$

$$G_{1111} = G_{115} + G_{119} + G_{11c} \tag{63}$$

$$G_{1212} = G_{1213} + G_{123} \tag{64}$$

$$G_{1313} = G_{137} + G_{1312} \tag{65}$$

### 2.2 The Steady State Analysis

Equation (23) holds firm for the induction motor when it is rotating. However, at stand still, a different conductance matrix  $[G_{ts}]$  is used because of the attendant change in the value of the convective elements of the branch thermal impedances. The stand still equation when there is no supply (no heat generation), is given as  $[C] \frac{d[T]}{dt} = [P_t] - [G_{ts}][T]$  (66)

During the steady state, the thermal capacitance is at maximum so that the derivative  $\frac{d[T]}{dt} = 0$  hence misses its contribution just as it renders equation (21) as  $P_a = \sum_{b=1}^N \left( \frac{T_a - T_b}{R_{a,b}} \right)$   $a = 1 \dots N$  (67)

Hence the algebraic steady-state temperature rise in the proposed thermal network model in matrix form can be written as follows:  $[P_t] = [G_t][T_t]$  (68)

So that we have on arranging that  $[T_t] = [G_t]^{-1}[P_t]$  (69)

where all the three variables are as defined thus;

With  $G_{11}, G_{22} \dots \dots \dots G_{NN}$  taking their usual values, the results of the simulated work are presented in explicit form in table 1 for the different model configurations (a-d) and also shown in graphical forms. In the simulation, the temperature vector  $T_T$  which is given by  $T_T = [T_1 \ T_2 \ T_3 \ T_4 \ \dots \ T_N]^t$  is used instead of the temperature rise vector  $T$ . The first node is taken as ambient temperature and is reorganized by updating, during the simulation so as to get the transient solution from

$$[C_a] \frac{d[T_a]}{dt} = P_a - \frac{T_a}{R_{a,a}} + \sum_{b=1}^N \left( \frac{T_b}{R_{a,b}} \right) \quad a = 1 \dots N \tag{70}$$

This in matrix form appears in compact form as  $C \frac{dT}{dt} = P - GT$  (71)

**Table 1 - Steady State predicted temperatures {SSPT} values for: (A) LIM full model (B) LIM half model (C) SIM full model and (D) SIM half model**

Frame	Stator lamination	Stator winding	End-windingR	Rotor iron	Rotor winding	End-ringR	* Ambient	End-ringL	End-windingL	Stator teeth	Rotor teeth	
SSPT ( °C) for LIM A-FULL and B-HALF MODELS												
A	61.124	76.403	74.146	83.248	83.003	83.690	78.073	21.403	56.043	82.251	76.751	82.917
B	58.701	73.078	69.144	78.662	78.163	75.677	70.014	21.241	-	-	71.773	78.075
SSPT ( °C) for SIM C-FULL and D- HALF MODELS												
C	61.510	76.928	78.942	80.845	68.550	68.248	63.856	21.161	63.856	80.845	-	-
D	62.504	78.297	79.908	81.735	74.729	74.580	69.547	21.258	-	-	-	-

\* Not shown on the graph

### 3. Machine Parameters

The parameters of the machine and other constants used are presented in table 2.

**Table 2 - Machine Parameters and geometric dimension [3, 5]**

Machine elements	Values
Height of slot	16.9 mm
Width of slot	7.76 mm
Length of air-gap between slot teeth and insulation	0.1 mm
Thickness of insulation	0.2 mm
Area of conductor at the end-winding	40.38 mm <sup>2</sup>
Length of end-winding connection	216.79 mm
Height of stator iron teeth	17.5 mm
Number of rotor slots	28
Outer radius of stator	100 mm
Inner radius of stator	62.5 mm
Base of rotor slot	4.06 mm
Slot-die ratio	1:12
Thickness of slot insulation	0.3 mm
Inner radius of rotor	15 mm
Height of end-ring	13.2 mm
Width of end-ring	4.4 mm
Copper winding cross section in slots	40.38 mm <sup>2</sup>
Iron core length	170 mm
Total slot length	239 mm
Length of rotor bar for sectioning	12.144 mm
Mean roughness of air-gap	3e-7 m
Air- gap length between stator core and lamination	0.7 mm
Width of bar	3.86 mm
Area of insulation	2570.4 cm <sup>2</sup>
Thickness of air	0.001mm
Radius of end-ring	2.03 mm
Height of rotor bar	13.7 mm
Length of frame	250 mm
Radius of frame	135 mm
Number of end-caps	40
Number of rotor slots	28
Coil pitch	12
Diameter of wire	0.71mm
Height of end-ring	13.2mm
Width of end-ring	4.4mm
Length of half-turn of stator winding	39.667 mm
Equivalent stacking factor for rotor and stator	0.95
Permeability of free space	$4\pi \times 10^{-7}$ H/m
Temperature coefficient of copper at 20 <sup>0</sup> C	0.0039 /K
Number of turns in the stator winding	174
Specific heat capacity $C_{cu} = 385J / kg.K, C_{fe} = 460J / kg.K, C_{endR} = C_{frame} = 960J / kg.K$	
Thermal conductivity $k_{cu} = 3.8W / Cm.K, k_{fe} = 0.5W / Cm.K, k_{ins} = 2 \times 10^{-3}W / Cm.K$	
Density $\rho_{cu} = 8900Kg / m^3, \rho_{fe} = 7800Kg / m^3, \rho_{endR} = \rho_{frame} = 2650Kg / m^3$	

### 3.1 Graphical Presentation

The response graphs from the simulations are presented as follows:

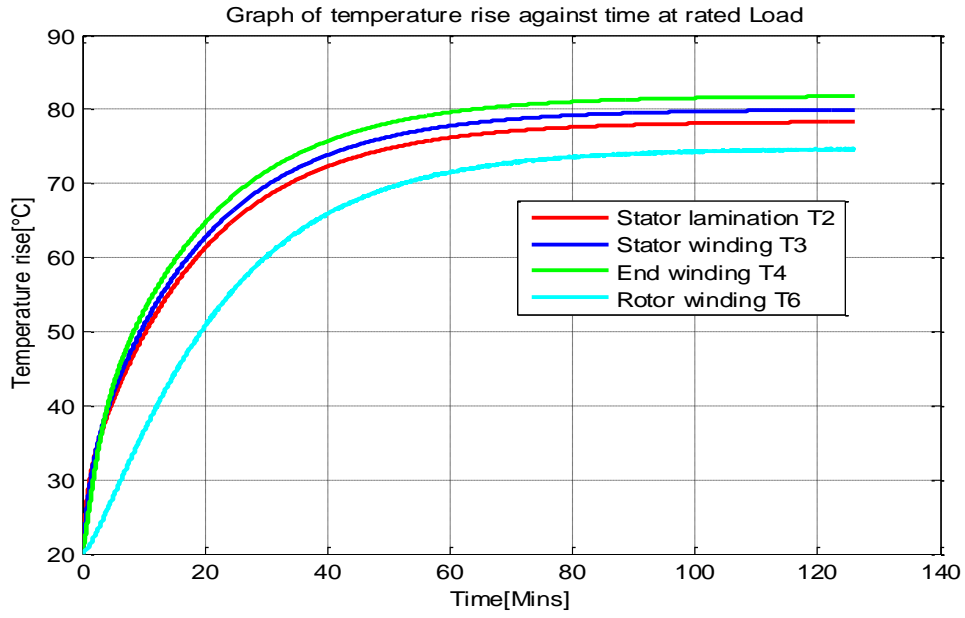


Fig. 5 - Response curve for the predicted temperatures- half SIM model

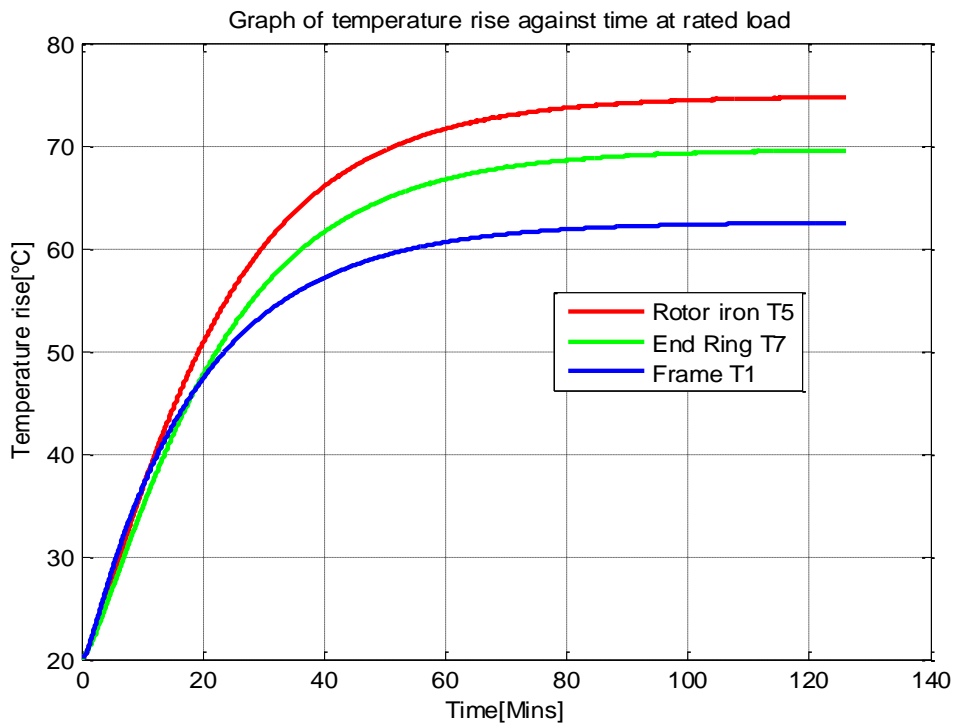
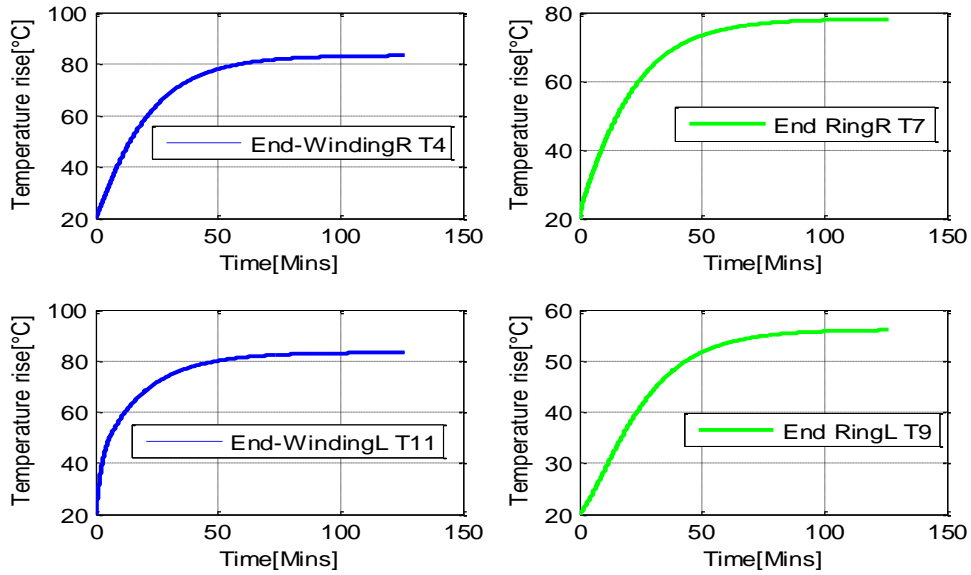
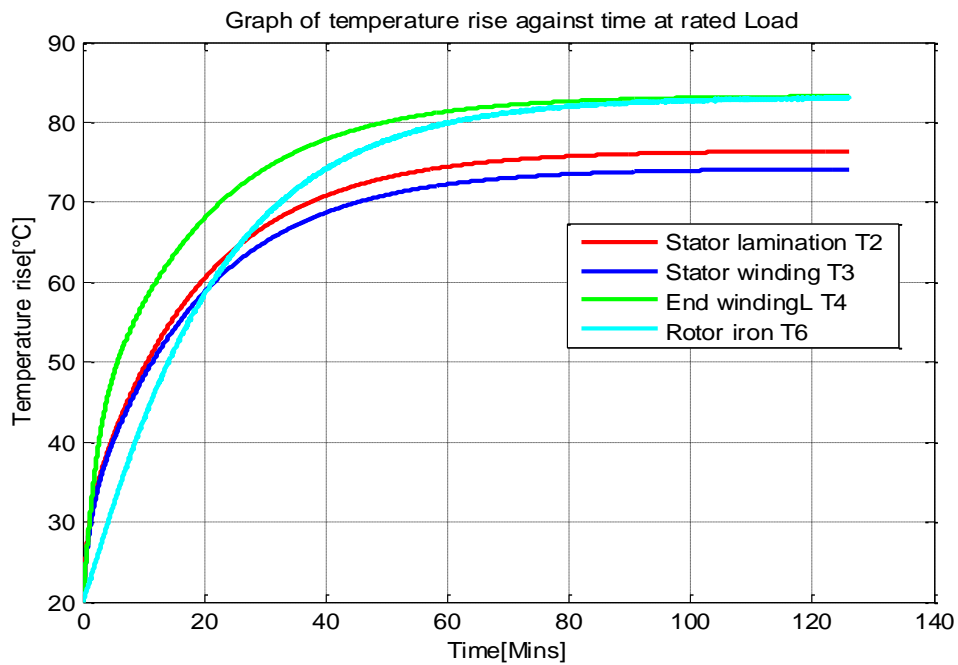


Fig. 6 - Response curve for the predicted temperatures-half SIM model continued



**Fig. 7 - Response curve for predicted temperature and symmetry for full SIM**



**Fig. 8 - Response curve for the predicted steady state temperatures for LIM**

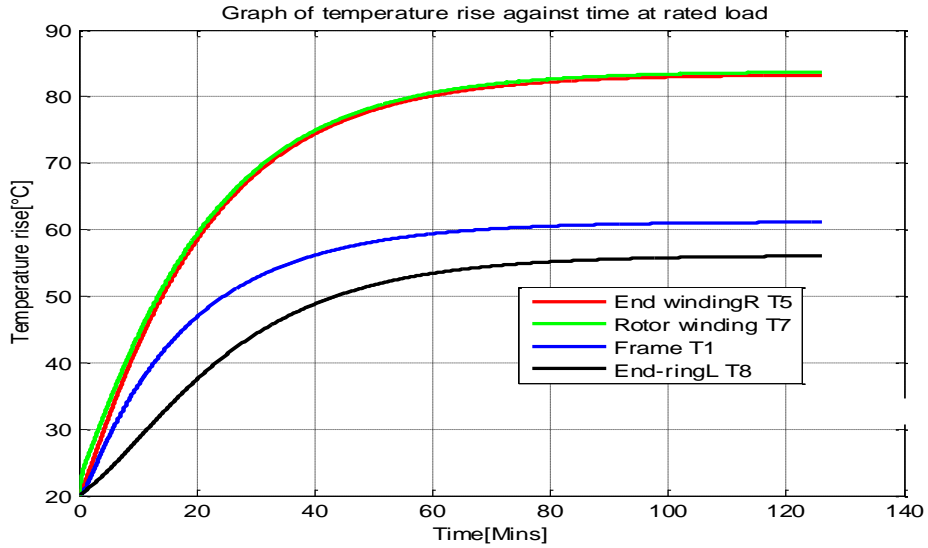


Fig. 9 - Response curve for the predicted temperatures for LIM continued

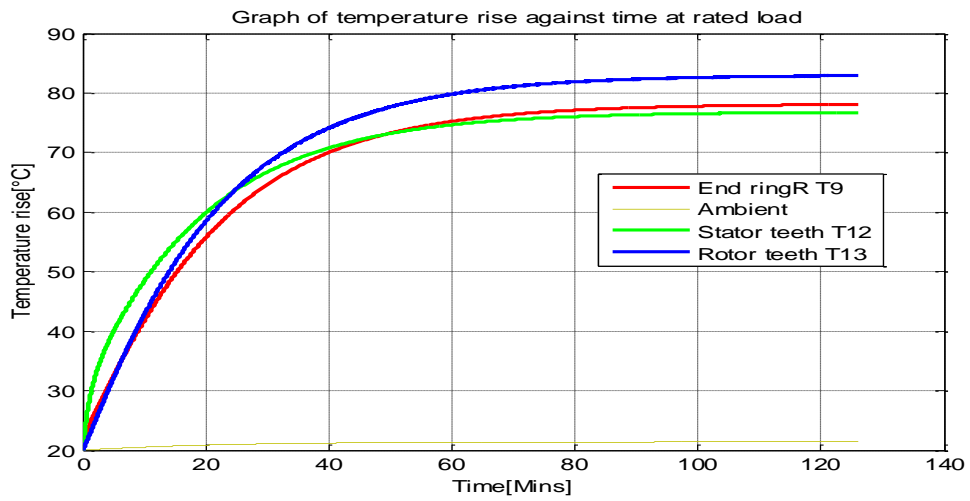


Fig. 10 - Response curves for the predicted steady state temperature rise for LIM continued

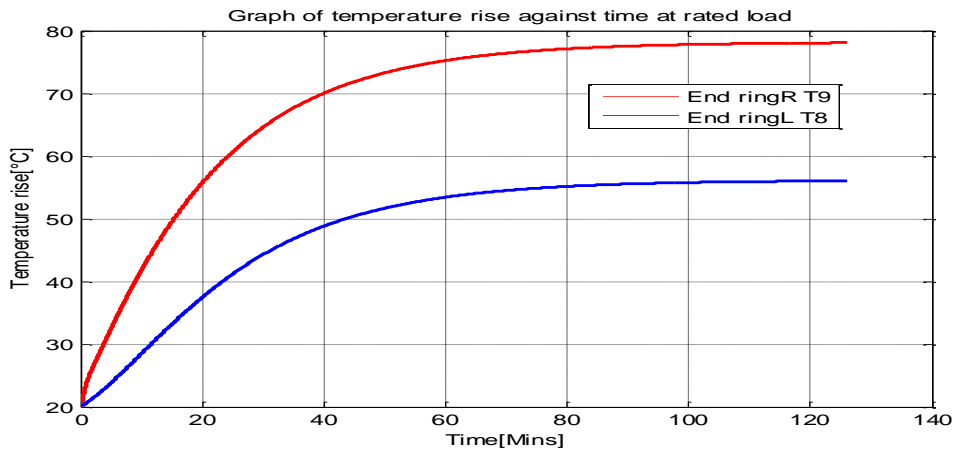
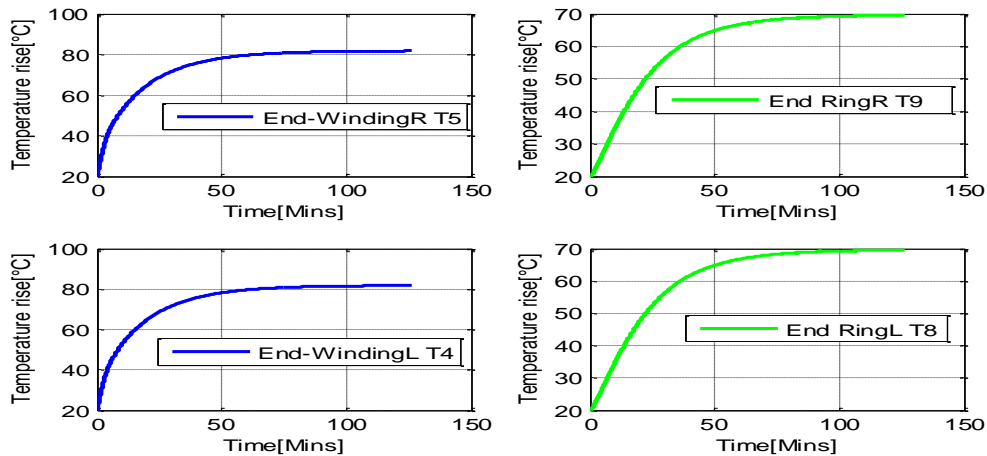


Fig. 11 - Comparing the response curves to show extent of difference in symmetry in end-ring of LIM model



**Fig. 12 - Response curve for predicted temperature and symmetry for full LIM models**

### 3 Discussion of Results

It is obvious from table 1(D) representing SIM half model that the predicted steady state temperature values recorded are slightly less than that obtained from table 1(C) representing SIM full model. However, in table 1(C), the predicted steady state temperature values recorded for SIM full model shows that thermal symmetry effect was at play. This is easily noticed when end ring and end winding steady state temperature values are considered. From table 1(B) representing LIM half model, the predicted steady state temperature values recorded are also less than that obtained from table 1(A) representing LIM full model with that of left end ring giving a reasonable difference. In table 1(A), the predicted steady state temperature values recorded for LIM full model shows that the effect of thermal symmetry cannot be noticed again. This is easily observed when end ring, end winding, stator teeth and rotor teeth steady state temperature values are considered. Hence, as the machine grows in size, the lesser the thermal influence on the symmetry configuration.

In figures 5 and 6, the response curves showing the predicted temperature rise for the machine (LIM) core parts are shown. Figure 7 shows the response curve for predicted temperature for full SIM model showing the symmetry effect. It is observed that the left and right parts of the machine core parts exhibited the same graphical characteristics showing good symmetry. This is not the same with the LIM model as is evident in table 1(B). Figures 8–11 present the response curve for predicted temperature for LIM model. While the predicted temperature rise is relatively small for the left end-ring and the frame part, the end winding, the rotor teeth and the rotor iron showed a remarkable increase with the end-winding showing the highest value. Figures 11 and 12 are there for the comparison of response curve for predicted temperatures for LIM and SIM models in terms of symmetry effect. It is just clear that unlike in the case of SIM, there is no associated symmetry exhibited in the LIM configuration.

### 4 Conclusion

In the work presented so far, the need for thermally modelling a system such as this machine is highlighted. The basics of the thermal modelling are introduced and the general equation for the implementation obtained. The calculation of thermal capacitances, thermal resistances and the consideration of losses all led to the determination of the thermal conditions of the core parts. For the full nodal configuration, the predicted temperature rise in degree centigrade for the core parts of the machine are as follows: frame (61.51), stator lamination (76.93), stator winding (79.94), end-windingR (80.85), rotor iron (68.55), rotor winding (68.25), end-ringR (63.86), end-ringL (63.86) and end-windingL (80.85) for SIM model and frame (61.13), stator lamination (76.40), stator winding (74.15), end-windingR (83.25), rotor iron (83.00), rotor winding (83.69), end-ringR (78.07), end-ringL (56.04), end-windingL (82.25), stator teeth (76.75), rotor teeth (82.92) for LIM model. It is observed that contrary to the research results of some authors, the machine does not have a uniform increase in temperature in some of the core parts due to symmetry. The larger the machine, the more the difference in temperature meaning reduced symmetry effect. The transient and steady state models are analysed. Tabular and graphical results from the steady state simulation are presented leading to a clearer comparison of results obtained. Finally, this work can appropriately be employed to predict the temperature distribution in a temperature sensitive induction machine for wind energy generation. In general terms, the results obtained in this may serve as useful information to motor designers and the industry especially on the thermal characteristics of the induction machine.

## References

- [1] Boglietti, A. Cavagnino and D. Staton, Evolution and Modern Approaches for Thermal Analysis of Electrical Machines, IEEE transactions on Industrial Electronics, vol. 56, no. 3, March 2009, pp. 871-882
- [2] C. Hwang, P. Tang, and Y. Jiang, "Thermal analysis of high-frequency transformers using finite elements coupled with temperature rise method," IEE Proceedings on Electric Power Applications, vol. 152, no. 4, pp. 832 – 836, 2005
- [3] G. Kylander, Thermal modelling of small cage induction motors, Technical Report no 265, Chalmers University of Technology, Gothenburg, Sweden, p. 113, 1995
- [4] O.I. Okoro, Bernd Weidemann, Olorunfemi Ojo, "An efficient thermal model for induction machines", Proceedings of IEEE Transactions on Industry and Energy conversion, Vol.5, No.4, pp. 2477-2484, 2004
- [5] S.E.Oti , E.J. Akpama, D.B.N. Nnadi; Thermal Analysis of a Transformer as an Electrical Machine, International Journal of Engineering and Management Research, Volume-6, Issue-5, September-October 2016, pp 70-75
- [6] N. Arabab, W. Wang, C. Lin, J. Hearron, B. Fahimi, Thermal modelling and analysis of a double-stator switched reluctance motor. IEEE Transaction on Energy Conversion 2015, 30, 1209–1217
- [7] W. Jang, T.M. Jahns, Coupled electromagnetic-Thermal analysis of electric machine including transient operation based on finite element techniques. IEEE Transaction on Industry and Application 2015, 51, 1880–1889
- [8] X. Liu, H. Yu, Z. Shi, Electromagnetic-fluid-thermal field Calculation and analysis of a permanent magnet linear motor. In Proceedings of the 2016 IEEE Conference on Electromagnetic Field Computation (CEFC), Miami, FL, USA, 13–16 November, 2016
- [9] Y. Xie , J. Guo, P. Chen and Z. Li, Coupled Fluid-Thermal Analysis for Induction Motors with Broken Bars Operating under the Rated Load, Energies Journal, (MDPI), 2018, pp.1-17
- [10] S.E. Oti, Ugwu J. , Nnadi D. B. , Ogbuefi U., Development and thermal modeling of an induction machine, International Journal of Engineering & Technology, 8 (4) (2019), pp.500-508
- [11] A. Boglietti, A. Cavagnino, M. Parvis, and A. Vallan, "Evaluation of radiation thermal resistances in industrial motors," IEEE Trans. Ind. Appl., vol. 42, no. 3, pp. 688–693, May 2006
- [12] L. Sang-Bin, T.G. Habetler, G. Ronald and J. D. Gritter, "An Evaluation of Model-Based Stator Resistance Estimation for Induction Motor Stator Winding Temperature Monitoring", IEEE Transactions on Energy Conversion, Vol.17, No.1 pp. 7-15, March 2002
- [13] O.I. Okoro, "Simplified Thermal Analysis of Asynchronous Machine", Journal of ASTM International, Vol.2, No.1, pp. 1- 20, January 2005
- [14] P. S. Ghahfarokhi, A. Kallaste, A. Belahcen and T. Vaimann, Steady State and Transient Thermal Analysis of the Stator Coil of a Permanent Magnet Generator, European Power Electronics Conference, May 2017. DOI: 10.1109/EPE.2017.7967242
- [15] S.E. Oti, D.B.N. Nnadi, C. A Nwosu., Fundamentals of Thermal Modelling of Induction Machines, International Conference on Electric Power Engineering (ICEPENG 2015) October 14-16, 2015 pp. 53- 55
- [16] P.H. Mellor, D. Roberts, D.R. Turner, "Lumped parameter model for electrical machines of TEFC design", IEEE Proceedings-B, Vol.138, No.5, pp. 205-218, September 1991
- [17] M.R. Feyzi and A.M. Parker, "Heating in deep-bar rotor cages", IEEE Proceedings on Electrical Power Applications, Vol.144, No.4, pp. 271-276 ,July 1997
- [18] S.J. Pickering, D. Lampard, M. Shanel,: "Modelling Ventilation and Cooling of Rotors of Salient Pole Machines," IEEE International Electric machines and Drives Conference (IEMDC), pp. 806-808, June 2001
- [19] C.M. Liao, C.L. Chen, T. Katcher,: "Thermal Management of AC Induction Motors Using Computational Fluid Dynamic Modelling," International Conference (IEMD '99) Electric machines and Drives, pp. 189-191, May 1999.
- [20] P.C. Krause and C.H. Thomas, "Simulation of symmetrical Induction machines," IEEE Transactions PAS-84, Vol.11, pp.1038-1053, 1965
- [21] F.J. Gieras, R. Wang, M. J. Kamper, Axial flux permanent magnet brushless machines. 2nd edition, Springer publisher, 2008
- [22] A. Benjan, Heat transfer dynamics, Wiley, New York, 1993
- [23] A. Di Gerlando and I. Vistoli, "Improved thermal modelling of induction motors for design purposes", IEEE Proceedings on Magnetics, pp. 381 – 386
- [24] O.I. Okoro, "Steady and transient states thermal analysis of induction machine at blocked rotor operation", European transactions on electrical power, 16: pp. 109-120, October 2006
- [25] O.I. Okoro, Introduction to Matlab/Simulink for Engineers and Scientists, 2<sup>nd</sup> edition, John Jacob's Classic Publishers Ltd, Enugu, Nigeria, January 2008
- [26] Learning Matlab 7 User's guide, Students' version: The Mathwork inc, Natic, December 2005
- [27] S.E. Lyshevski, Engineering and Scientific computations using Matlab, John Wiley & Sons Inc. Publications, New-Jersey, 2003